Title
Removal of Chromium and Arsenic from Water Using Polyol-Functionalized Porous Aromatic Frameworks

Journal
Journal of the American Chemical Society, 146(34)

ISSN
0002-7863

Authors
Uliana, Adam A
Pezoulas, Ethan R
Zakaria, N Isaac
et al.

Publication Date
2024-08-28

DOI
10.1021/jacs.4c05728

JACS
JOURNAL OF THE AMERICAN CHEMICAL SOCIETY

pubs.acs.org/JACS
Article

Removal of Chromium and Arsenic from Water Using Polyol-Functionalized Porous Aromatic Frameworks

Adam A. Uliana, Ethan R. Pezoulas, N. Isaac Zakaria, Arun S. Johnson, Alex Smith, Yubing Lu, Yusuf Shaidu, Ever O. Velasquez, Megan N. Jackson, Monika Blum, Jeffrey B. Neaton, Junko Yano, and Jeffrey R. Long*

Cite This: J. Am. Chem. Soc. 2024, 146, 23831−23841

Read Online

ACCESS | Metrics & More | Article Recommendations | Supporting Information

ABSTRACT: Chromium and arsenic are two of the most problematic water pollutants due to their high toxicity and prevalence in various water streams. While adsorption and ion-exchange processes have been applied for the efficient removal of numerous toxic contaminants, including heavy metals, from water, these technologies display relatively low overall performances and stabilities for the remediation of chromium and arsenic oxyanions. This work presents the use of polyol-functionalized porous aromatic framework (PAF) adsorbent materials that use chelation, ion-exchange, redox activity, and hydrogen-bonding interactions for the highly selective capture of chromium and arsenic from water. The chromium and arsenic binding mechanisms within these materials are probed using an array of characterization techniques, including X-ray absorption and X-ray photoelectron spectroscopies. Adsorption studies reveal that the functionalized porous aromatic frameworks (PAFs) achieve selective, near-instantaneous (reaching equilibrium capacity within 10 s), and high-capacity (2.5 mmol/g) binding performances owing to their targeted chemistries, high porosities, and high functional group loadings. Cycling tests further demonstrate that the top-performing PAF material can be recycled using mild acid and base washes without any measurable performance loss over at least ten adsorption−desorption cycles. Finally, we establish chemical design principles enabling the selective removal of chromium, arsenic, and boron from water. To achieve this, we show that PAFs appended with analogous binding groups exhibit differences in adsorption behavior, revealing the importance of binding group length and chemical identity.

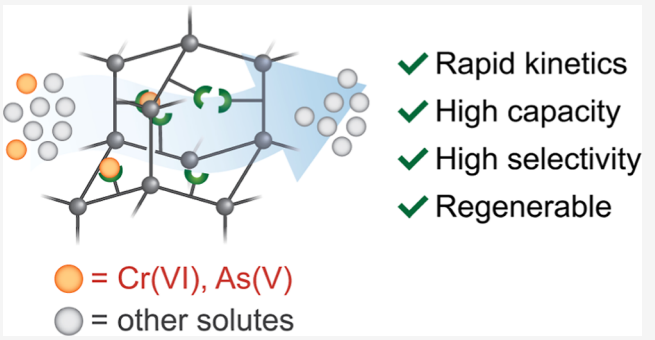

INTRODUCTION

Although water is the most abundant resource on Earth, it is estimated that one-quarter of the global population lacks water that is free from contamination.[1] The removal of micropollutants (e.g., heavy metals) from water is one of the most pressing yet technologically difficult water treatment challenges worldwide. These contaminants are often found in various water sources at trace yet toxic concentrations, alongside competing constituents of similar size and charge that are more concentrated yet relatively nontoxic (e.g., sodium chloride).[2,3] For example, chromium(VI)-based oxyanions have caused immense issues related to water contamination.[4] Such species are highly mutagenic and carcinogenic to living systems, yet are commonly released to the environment through industrial processes such as metallurgy, electroplating, mining, leather tanning, pigment production, and cement production.[5,6] As another damaging contaminant, arsenic is often present in natural groundwater in areas such as Bangladesh and lowland Amazonia at concentrations much higher than the drinking water limit endorsed by the World Health Organization (10 ppb).[7] This water contamination leads to an estimated 43,000 deaths per year caused by arsenic poisoning in Bangladesh alone.[8]

Various separation methods have been proposed to achieve selective chromium and arsenic removal from water, including ion-exchange,[4] adsorption,[9] membrane separations,[10−12] electrocoagulation,[13] and photocatalytic degradation.[14] Of these methods, adsorption and ion-exchange are often considered as among the most promising due to their low operating and capital costs, high uptake capacities, and ease of use.[10] Adsorbents and ion-exchange resins consist of an inorganic material (e.g., zeolites, layered double hydroxides, metal oxides) or organic polymer. These materials are cost-effective but typically exhibit poor sorption kinetics, chemical and thermal stability, and/or recyclability.[4,15] Moreover, these

Received: April 26, 2024
Revised: August 7, 2024
Accepted: August 7, 2024
Published: August 16, 2024

methods generally rely on leveraging electrostatic interactions (e.g., ion-exchange) that exhibit relatively low selectivity for chromium and arsenic oxyanions over other common waterborne anions.[4,9] These drawbacks necessitate the development of robust materials and methods that can more effectively achieve chromium and arsenic oxyanion separations.

In this work, we sought to address the limitations of existing adsorption and ion-exchange methods by developing methods based on the use of functionalized porous aromatic frameworks (PAFs). PAFs are a class of porous network polymers that feature a highly porous, diamondoid-like structure composed of organic nodes covalently and irreversibly coupled through aromatic linkages.[16,17] As a result, PAFs display exceptional hydrothermal and chemical stabilities, such as stability in boiling water, concentrated acids and bases, and organic solvents.[17−19] Functionalization of the organic struts within these framework materials can lead to specific molecular interactions that enable the high-capacity removal of a variety of targeted ions from water.[20−23]

Here, we show that PAFs functionalized with the aminopolyol *N*-methyl-D-glucamine (NMDG) capture chromium from water through selective and redox-active diol chelation interactions, with unprecedented uptake rates, high adsorption capacities, and stable cycling performance. These adsorbent materials additionally capture arsenic rapidly through selective hydrogen-bonding and ion-exchange interactions. Previous reports have described the use of aminopolyols and diols in macroporous polymeric materials to achieve chromium and arsenic capture,[24−28] but their precise adsorption mechanisms have not been elucidated. Additionally, owing to their low porosities and poor synthetic tunability, these materials show limited capacities, uptake rates, and stabilities. Other material classes with higher porosities and extensive tunability (e.g., metal−organic frameworks) have been reported as alternative adsorbents for chromium and arsenic oxyanion capture. However, these reported materials have typically relied on electrostatic ion-exchange interactions between the oxyanions and cationic groups on the material, leading to relatively low selectivity over other waterborne anions.[4,29−31]

RESULTS AND DISCUSSION

Design, Synthesis, and Structural Characterization. The parent PAF-1 framework, which consists of tetrahedral carbon nodes connected by biphenyl struts (Figure 1a), was synthesized through a Yamamoto-type Ullmann coupling reaction starting with the monomer tetrakis(4-bromophenyl)-methane.[16] The NMDG functional group was then appended onto the framework through a facile two-step route, starting with the chloromethylation of PAF-1 before the subsequent nucleophilic addition of NMDG.[22] To investigate the effects of aminopolyol size, diol positioning, and ammonium counter-anion-exchange, this synthetic strategy was also implemented to synthesize three new frameworks (PAF-1-MAPD, PAF-1-serinol, PAF-1-N$(CH_3)_2$) containing methylamino-1,2-propanediol (MAPD, featuring a 1,2-diol), serinol (featuring a 1,3-diol), or dimethylamine functional groups, respectively (Figure 1). Notably, PAF-1-N$(CH_3)_2$ acts as a weak base anion-exchange resin without alcohol functionalities.

The successful syntheses of these materials were verified by elemental analysis, Fourier-transform infrared spectroscopy (FTIR), surface area measurements, and thermogravimetric analyses. For each aminopolyol- or amine-functionalized material, elemental analyses revealed an increase in nitrogen

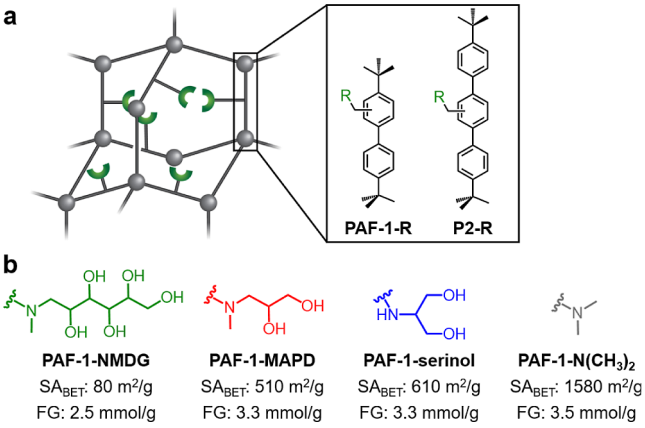

Figure 1. (a) Schematic of functionalized PAF pores used in this work, where R indicates an appended functional group. (b) Functional groups appended onto PAFs in this work, along with the corresponding names of the resulting materials. NMDG: *N*-methyl-D-glucamine, MAPD: 3-methylamino-1,2-propanediol, SA$_{BET}$: Brunauer−Emmett−Teller specific surface area, FG: functional group loading per gram of functionalized PAF material.

content close to the values expected for a loading of one functional group per biphenyl strut (see Supporting Information). Based on these nitrogen elemental analyses, the functional group loadings were calculated to be 2.50, 3.29, 3.27, and 3.51 mmol/g for PAF-1-NMDG, PAF-1-MAPD, PAF-1-serinol, and PAF-1-N$(CH_3)_2$, respectively (Figure 1b and Table S1). The FTIR spectra of PAF-1-NMDG, PAF-1-MAPD, and PAF-1-serinol showed the appearance of new peaks at 1040, 1080, and 3300−3500 (broad) cm^{-1}, corresponding to C−O, C−N, and O−H bonds on the aminopolyols, respectively (Figure S2).[22,32] These spectra also showed the disappearance of the peak at 1260 cm^{-1}, corresponding to the C−H wagging mode of −CH_2Cl on the PAF-1-CH_2Cl precursor.[21,32]

Nitrogen adsorption isotherms were collected at 77 K for the functionalized PAFs to determine their Brunauer−Emmett−Teller (BET) surface areas (Figures S3 and S4). The obtained BET surface areas for PAF-1, PAF-1-CH_2Cl, PAF-1-N$(CH_3)_2$, PAF-1-serinol, PAF-1-MAPD, and PAF-1-NMDG were found to be 4530, 1950, 1580, 610, 510, and 80 m^2/g, respectively. We note that decreases in surface area upon incorporation of functional groups into PAF-1 are consistent with previous reports and are likely due to the partial pore filling and the added mass of the functional groups.[19−21,33] Nonetheless, the relatively high surface areas of the functionalized PAFs suggest high accessibility of the functional groups within the frameworks, as well as high porosities for these materials.[20] Furthermore, thermogravimetric analysis (TGA) decomposition results indicate high thermal stability of the materials (no decomposition below 200 °C), along with expected drops in mass in the range 200−500 °C that are consistent with the masses of the functional groups (Figure S7).

Equilibrium Cr(VI) and As(V) Adsorption Properties. We then examined the Cr(VI) adsorption properties of the four synthesized PAF materials. Importantly, the amine on each functional group is predicted to have a pK_a near or above 9, causing these functional groups to be protonated at neutral pH conditions. Simulations performed using HySS software[34] also indicate that Cr(VI) exists completely in the oxyanion

https://doi.org/10.1021/jacs.4c05728
J. Am. Chem. Soc. 2024, 146, 23831−23841

state at neutral pH conditions in our measurements, with the predominant species being CrO_4^{2-} (Figure S9). Thus, each framework can potentially participate in anion-exchange interactions with the oxyanions, while PAF-1-NMDG, PAF-1-MAPD, and PAF-1-serinol also contain polyol groups that may additionally participate in Cr(VI) binding.

We first collected Cr(VI) adsorption isotherms and fit the resulting data to a single-site Langmuir model (Figures 2 and S18). High Cr(VI) saturation capacities were observed for each material: 2.50, 3.63, 3.70, and 2.87 mmol/g for PAF-1-NMDG, PAF-1-MAPD, PAF-1-serinol, and PAF-1-N$(CH_3)_2$, respectively. These capacities suggest that the functional groups bind Cr(VI) in a ~1:1 stoichiometric fashion (Table S2). Interestingly, further inspection in the low-concentration region of these isotherms reveals that PAF-1-NMDG captures Cr(VI) much more effectively than the other frameworks at dilute Cr(VI) concentrations, as indicated by a markedly steeper isotherm profile in this region (Figure 2 inset). Indeed, when applied to aqueous solutions containing 0.5, 1, or 5 ppm of Cr(VI), PAF-1-NMDG reduces the Cr(VI) to concentrations far below the 0.1 ppm maximum contaminant level for drinking water imposed by the U.S. Environmental Protection Agency (Figure S14).[35]

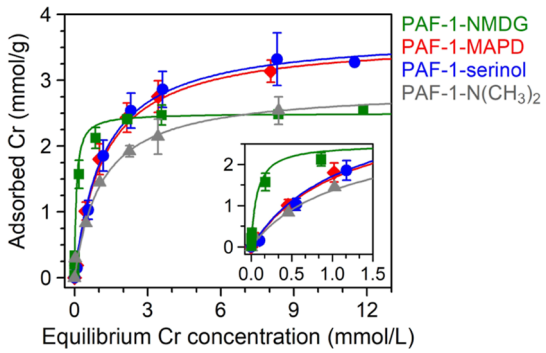

Figure 2. Chromium(VI) adsorption isotherms by PAF-1-NMDG (green squares), PAF-1-MAPD (red diamonds), PAF-1-serinol (blue circles), and PAF-1-N$(CH_3)_2$ (gray triangles). (Inset) Zoom-in of the dilute region of the isotherms. The adsorption data were fit by a single-site Langmuir model (solid lines). Error bars represent the standard deviation obtained from at least three replicate tests. The mean values obtained at each concentration are shown.

The Langmuir constant (K_L) obtained from the Langmuir model serves as a measure of equilibrium binding affinity.[36,37] The K_L value for Cr(VI) obtained for PAF-1-NMDG (14.4 L/mmol) was over an order of magnitude higher than those for PAF-1-MAPD (0.8 L/mmol), PAF-1-serinol (0.9 L/mmol), and PAF-1-N$(CH_3)_2$ (0.9 L/mmol) (Table S2). These differences confirm the higher Cr(VI) binding strength toward the NMDG functional groups than to the MAPD, serinol, and dimethylamine groups. The nearly identical K_L values among PAF-1-MAPD, PAF-1-serinol, and PAF-1-N$(CH_3)_2$ also suggest that Cr(VI) binding in each of these three frameworks occurs through a similar mechanism. Given that PAF-1-N$(CH_3)_2$ can only capture Cr(VI) oxyanions through anion-exchange interactions, these results suggest that PAF-1-MAPD and PAF-1-serinol also capture Cr(VI) via anion-exchange. Indeed, images of these three frameworks after Cr(VI) loading show that the frameworks gain a yellow-brown color upon adsorption (Figure S24), similar to the colors of Cr(VI) in solution and of Cr(VI)-loaded anion-exchange materials.[4,38] In contrast, PAF-1-NMDG turns a distinct green color upon Cr(VI) adsorption (Figure S24), suggesting significant changes to the CrO_4^{2-} coordination sphere and/or oxidation state upon adsorption.[39,40] These findings indicate that the additional length, flexibility, and/or number of alcohols present on NMDG facilitates the stronger Cr(VI) binding compared to the other synthesized adsorbents.

The high Cr(VI) loadings of these frameworks encouraged us to also explore their arsenic removal capabilities. Like Cr(VI), toxic As(V) generally exists fully in the oxyanion state at neutral pH conditions, predominantly as a mixture of $H_2AsO_4^-$ and $HAsO_4^{2-}$ ($pK_a \approx 7.0$).[41−43] The As(V) adsorption isotherms and their single-site Langmuir model fits revealed saturation capacities of 1.14, 0.93, 0.53, and 1.86 mmol/g for PAF-1-NMDG, PAF-1-MAPD, PAF-1-serinol, and PAF-1-N$(CH_3)_2$, respectively (Figures 3a and S19 and Table S3). These capacities suggest that approximately one As(V) binds to every two NMDG or dimethylamine functional groups. The associated K_L value for PAF-1-NMDG (2.2) was approximately double the values for PAF-1-MAPD (1.0) and PAF-1-N$(CH_3)_2$ (1.2) and four times the value for PAF-1-serinol (0.5), indicating a higher affinity for As(V). The similar K_L values obtained for PAF-1-MAPD and PAF-1-N$(CH_3)_2$ suggest that PAF-1-MAPD captures As(V) solely through anion-exchange interactions.

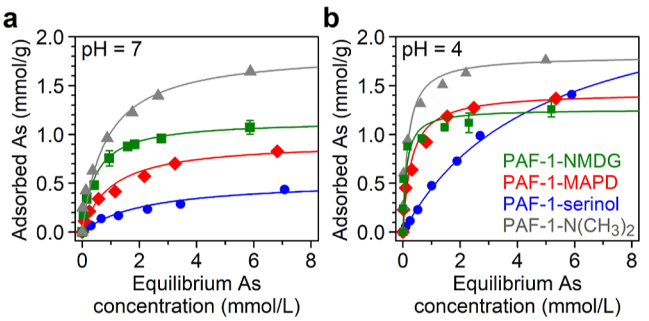

Figure 3. Arsenic(V) adsorption isotherms by PAF-1-NMDG (green squares), PAF-1-MAPD (red diamonds), PAF-1-serinol (blue circles), and PAF-1-N$(CH_3)_2$ (gray triangles), at (a) pH = 7 and (b) pH = 4 conditions as adjusted by HCl. The adsorption data were fitted by a single-site Langmuir model (solid lines).

Isotherms collected at pH = 4 conditions showed steeper adsorption profiles for each framework but otherwise similar saturation capacities and K_L differences among the frameworks, with the exception of PAF-1-serinol (Figures 3b and S20 and Table S4). At these conditions, As(V) predominantly exists as $H_2AsO_4^-$, potentially leading to more favorable binding due to the additional hydrogen bonding interactions that can engage this oxyanion species.[41−43] The exact mechanisms that lead to weaker binding in PAF-1-serinol compared to PAF-1-MAPD, indicated by the lower As(V) K_L values for PAF-1-serinol, are still under investigation. However, these results suggest that the diol positioning and/or number of carbons bonded to the nitrogen affect As(V) adsorption properties. Cr(VI) and As(V) isotherms collected for unfunctionalized PAF-1 showed negligible adsorption (Figure S11), confirming that the PAF backbone does not facilitate adsorption.

Mechanisms of Cr(VI) and As(V) Adsorption. We employed X-ray absorption spectroscopy (XAS) to elucidate the rapid and strong Cr(VI) and As(V) binding mechanisms of PAF-1-NMDG. We first leveraged X-ray absorption near-edge

https://doi.org/10.1021/jacs.4c05728
J. Am. Chem. Soc. 2024, 146, 23831−23841

structure (XANES) spectroscopy at the Cr K-edge to probe the electronic structure of the bound Cr (Figure 4a, inset).

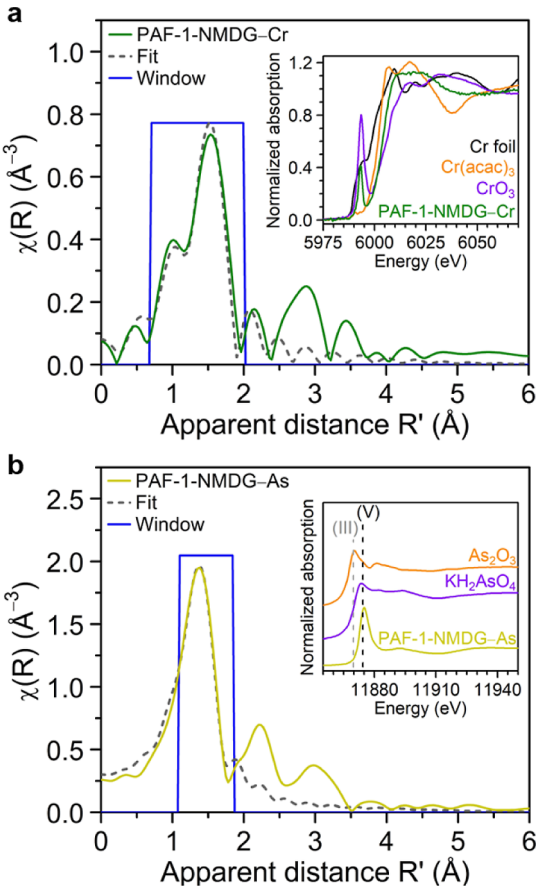

Figure 4. Fourier-transformed extended X-ray absorption fine structure (EXAFS) spectra and the one-shell fitting results for (a) Cr(VI)- and (b) As(V)-loaded PAF-1-NMDG. Phase shifts are not included in the displayed apparent distances. (Insets) XANES spectra for each respective sample.

However, the features of the Cr K-edge XANES spectrum of Cr(VI)-dosed PAF-1-NMDG are ambiguous. While the pre-edge feature at 5993 eV is aligned with a feature commonly used to fingerprint formally Cr(VI) species,[44] such as CrO_3, the main edge position at approximately 6011 eV is within 5 eV of the main edge of Cr(acac)$_3$ (acac$^-$ = acetylacetonate) and other compounds featuring exclusively octahedral Cr(III) sites.[45]

In contrast, oxidation state assignment based on the As K-edge XANES data for As-loaded PAF-1-NMDG is more straightforward. The white-line position at 11,875 eV is well-aligned with that of KH_2AsO_4 at 11,873 eV (Figure 4b, inset), consistent with the expected white-line range for As(V)-containing compounds[46] and strongly supporting the assignment of a +5 As oxidation state. Thus, the XANES data suggest that the primary As(V) adsorption mechanism by PAF-1-NMDG is not As(V) reduction.

X-ray photoelectron spectroscopy (XPS) at the Cr 2p core level was conducted on Cr-loaded PAF-1-NMDG to supplement the XANES data and clarify the speciation of captured Cr (Figure 5). Deconvolution of the Cr 2p region reveals multiplet splitting at the 2p$_{3/2}$ peak (components 1 and 2 at 576.7 and 578.0 eV, respectively). Such multiplet splitting has

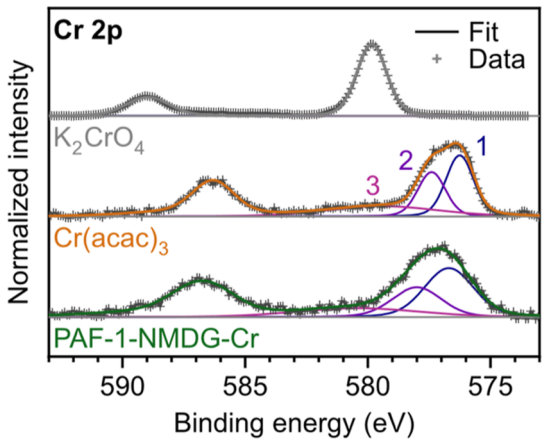

Figure 5. Chromium 2p XPS data for K_2CrO_4, Cr(acac)$_3$, and Cr(VI)-dosed PAF-1-NMDG. The latter two spectra were fitted by a five-component model (solid lines). For brevity, only the three components associated with the 2p$_{3/2}$ level are displayed. The components 1, 2, and 3 correspond to the main, spin−orbit splitting, and shakeup components of the 2p$_{3/2}$ level, respectively. The data for K_2CrO_4 were fit with a two-component model, wherein the lower-energy component corresponds to the 2p$_{3/2}$ level. Fit parameters are listed in Table S8.

been observed for other compounds with octahedral Cr(III) centers, such as Cr_2O_3 and Cr(acac)$_3$ (Figure S37).[47,48] The broad component at 580.4 eV (component 3) is assigned to shakeup structure that is also observed for Cr(acac)$_3$ and derivatives thereof.[48] Overall, the similar intrinsic loss structure apparent in the spectra of Cr-dosed PAF-1-NMDG and Cr(acac)$_3$ indicate that the mechanism for Cr(VI) capture in PAF-1-NMDG is dominated by the reduction of Cr(VI) to Cr(III), consistent with prior observations of alcohol oxidation by Cr(VI) species in certain acidic environments.[49] The oxidation of PAF-1-NMDG alcohols upon Cr binding is supported by FTIR and XPS (Figures S38−S40).

EXAFS spectroscopy was leveraged to confirm the coordination environment of Cr and As in the respective dosed PAF-1-NMDG samples. The fitted spectra for Cr and As are displayed in Figures 4a and S28 and 4b and S29, respectively. Fit parameters, including coordination numbers and bond lengths, are listed in Table 1. The fits indicate that Cr(III) forms a six-coordinate complex with PAF-1-NMDG upon adsorption, consisting of four Cr−O bonds with a 1.93 Å bond distance and two Cr−O bonds with a 1.63 Å bond distance. The coordination number increase of two for Cr compared to the starting four-coordinate CrO_4^{2-} species confirms the Cr coordination to the NMDG alcohol groups, in agreement with the Cr 2p XPS data. The Cr−O bond distance of 1.93 Å is remarkably similar to that found in Cr(acac)$_3$ (Cr−O bond distance of 1.95 Å),[50] suggesting the partial oxidation of the NMDG polyol. This, coupled with the similar XPS spectra of Cr(acac)$_3$ and Cr-loaded PAF-1-NMDG (Figure 5), support the potential bischelate Cr(III) structure proposed in Figure 6. In this structure, oxidized NMDG acts as an acetylacetonate analog, binding the Cr(III). While the Cr complex itself has a local charge of −1, this is balanced by the positively charged NMDG ammonium cation.

Fits for the As K-edge EXAFS spectrum showed that As(V) maintains four As−O bonds upon adsorption to PAF-1-NMDG, with bond distances (1.82 Å) elongated compared to those reported in the Cambridge Crystallographic Data Centre

https://doi.org/10.1021/jacs.4c05728
J. Am. Chem. Soc. 2024, 146, 23831−23841

Table 1. EXAFS Fitting Results of the Cr- (Unshaded) and As-Loaded (Shaded in gray) PAF-1-NMDG and PAF-1-N(CH_3)$_2$

material	path	N^a	R (Å)^b	σ^2 (Å^2)^c	ΔE_0 (eV)^d	R-factor (%)^e
PAF-1-NMDG−Cr	Cr−O	2	1.63 ± 0.02	0.005	−3.99 ± 7.94	1.8
	Cr−O	4	1.93 ± 0.04	0.005	−3.99 ± 7.94	1.8
PAF-1-N(CH_3)$_2$−Cr	Cr−O	4	1.59 ± 0.01	0.005	3.94 ± 1.95	0.8
PAF-1-NMDG−As	As−O	4	1.82 ± 0.02	0.005	5.57 ± 2.43	0.3
PAF-1-N(CH_3)$_2$−As	As−O	4	1.70 ± 0.01	0.001	6.21 ± 2.06	0.5

^{a}Coordination number. ^{b}Bond length. ^{c}Mean-square relative displacement (Debye−Waller factor). ^{d}Edge shift. ^{e}Goodness-of-fit parameter.

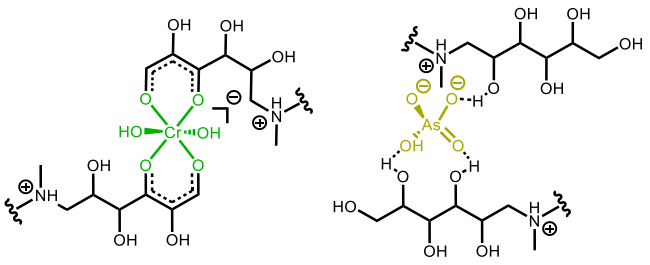

Figure 6. Proposed structures of Cr(III) (left) and As(V) (right) bound to PAF-1-NMDG.

for K_3AsO_4 (1.69 Å). While the exact causes for this bond elongation are still being investigated, we propose two potential As(V)-NMDG complex structures. In the first proposed structure (Figure 6), the As(V) oxyanion undergoes simultaneous anion-exchange to the protonated NMDG amine and hydrogen bonding to the polyol groups. These additional hydrogen bonding interactions may explain the improved affinity of As(V) toward PAF-1-NMDG compared to the anion-exchange-only PAF-1-N(CH_3)$_2$ and shorter-chain PAF-1-MAPD, as indicated by the previously described As(V) adsorption isotherms. The second proposed structure (Figure S35) features a monochelate mechanism, where two alcohols on one NMDG functional group chelate to one As(V) oxyanion.

Another method of probing the local coordination environments of Cr and As in PAF-1-NMDG would be through the crystallographic characterization of analogous molecular complexes. However, attempts to isolate crystalline benzyl aminopolyol complexes with Cr and As were unsuccessful.

For comparison, we also collected XANES spectra for Cr- and As-loaded PAF-1-N(CH_3)$_2$. The data reveal that these adsorbates maintain their +6 and +5 oxidation states upon adsorption, respectively, as expected for anion-exchange interactions (insets of Figures S32 and S33). The EXAFS fits also show that the Cr maintains four Cr−O bonds with a 1.59 Å bond distance upon adsorbing to PAF-1-N(CH_3)$_2$ (Figures S30 and S32 and Table 1), highly similar to the crystallographic structure reported for $Na_2CrO_4{\cdot}4H_2O$ (Cr−O distances: 1.64 Å).[51] Consistent with an anion-exchange mechanism, these similarities verify that the coordination sphere of Cr(VI) does not change upon CrO_4^{2-} adsorption in PAF-1-N(CH_3)$_2$, unlike in the case of adsorption in PAF-1-NMDG.

With this gained insight, we then wanted to better understand why the shorter aminopolyols MAPD and serinol do not achieve the high-affinity Cr(VI) oxyanion binding realized with PAF-1-NMDG. To do this, we investigated the $B(OH)_3$ adsorption properties of the three frameworks. Notably, unlike for chromium or arsenic separations, the NMDG functional group is used on an industrial scale to remove boric acid from water, primarily through proposed monochelate, tetradentate, and bischelate adsorption mechanisms.[22,52−54] The MAPD and serinol groups have not been adopted for such separations, although their lighter molecular weights could lead to higher gravimetric adsorption capacities than NMDG, should they be capable of participating in the same types of chelation interactions.

Previous studies of the NMDG-$B(OH)_3$ adsorption mechanism revealed that $B(OH)_3$ adsorption is dominated by tetradentate and bischelate binding (Figure S36). Meanwhile, only a small fraction of the adsorption capacity was attributed to monochelate binding mechanisms (Figure S36).[22] Due to the smaller polyol sizes of MAPD and serinol, these functional groups cannot participate in tetradentate binding. However, these functional groups can in principle participate in bischelate binding if pore spacing and functional group flexibility allow multiple functional groups to come in close enough proximity to bind to the same adsorbate molecule.

The collected $B(OH)_3$ isotherms show that PAF-1-NMDG achieves boron saturation capacities (2.01 mmol/g) that are roughly six times that of PAF-1-MAPD (0.33 mmol/g) and PAF-1-serinol (0.36 mmol/g) (Figure S10 and Table S5). The drastically lower loadings for the latter two frameworks correspond to only 1 $B(OH)_3$ adsorbed per every ∼10 MAPD or serinol groups within the PAF. Given that much higher $B(OH)_3$ loadings are afforded through bischelate interactions, as previously explained, these data suggest that bischelate $B(OH)_3$ interactions—and thus presumably also bischelate Cr and As(V) interactions—do not occur to a large extent in PAF-1-MAPD or PAF-1-serinol. The lower Cr(VI) and As(V) binding affinities observed for PAF-1-MAPD and PAF-1-serinol can thus likely be attributed to the lack of tetradentate and bischelate binding capabilities for these frameworks.

Along these lines, we also tested the $Si(OH)_4$ adsorption performance of PAF-1-NMDG as a function of pH (Figure S17). Silicon-based compounds pose significant industrial water treatment issues, arising from their propensity to cause scaling and the relative lack of available techniques that can selectively remove these compounds.[55] Given the oxygen-rich speciation of waterborne silicon, we postulated that the NMDG functional groups could potentially adsorb silicon via analogous chelating mechanisms as those observed for $B(OH)_3$ and Cr(VI) and As(V) oxyanions. Unfortunately, minimal Si uptake was observed at all tested pH values (pH range: 1−12). The highest Si uptake occurred at pH conditions of 9.5 and 12.0, likely because Si is largely anionic (as $SiO(OH)_3^-$ and/or $SiO_2(OH)_2^{2-}$) at these conditions, enabling some anion-exchange to the NMDG amine. We hypothesize that the ability of $B(OH)_3$ and Cr(VI) to increase in coordination number (e.g., to the four-coordinate tetrahedral borate anion upon adsorption, or the six-coordinate Cr(III) complex), along with the redox activity of Cr(VI), plays a crucial role in the binding

https://doi.org/10.1021/jacs.4c05728
J. Am. Chem. Soc. 2024, 146, 23831−23841

of these solutes by NMDG alcohol groups. Similar chemical interactions are lacking for $Si(OH)_4$.

These mechanistic findings offer important guidelines for the design of adsorptive functional groups for not just chromium and arsenic separations, but also for boric acid and silicon separations.

Kinetics, Selectivity, pH Dependency, and Recyclability Tests for Cr(VI) and As(V) Removal. Informed by the isotherm and mechanistic data provided above, we identified PAF-1-NMDG to be the most promising material for Cr(VI) and As(V) removal out of the four PAF-1-derived frameworks. We thus sought to systematically characterize the Cr(VI) and As(V) removal performances of PAF-1-NMDG, starting with adsorption kinetics measurements.

Adsorption kinetics are one of the most important properties of adsorbents, influencing factors such as throughput and required adsorbent bed sizes. We measured the adsorption kinetics of PAF-1-NMDG using separate solutions containing 250 mg/L of Cr(VI) (in the form of CrO_4^{2-}) or As(V) (in the form of $H_2AsO_4^-$/$HAsO_4^{2-}$). In both cases, PAF-1-NMDG exhibited exceptionally fast kinetics: the equilibrium saturation capacities for Cr(VI) and As(V) were reached by the time the first data point was collected (<10 s) (Figure 7). To the best of

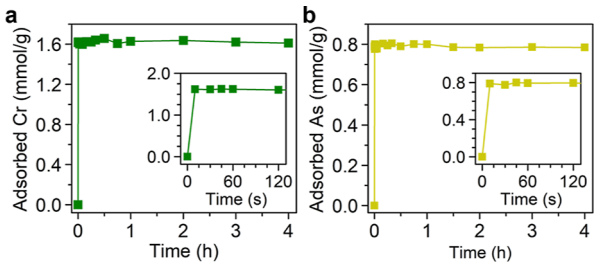

Figure 7. Adsorption kinetics for (a) Cr(VI) and (b) As(V) by PAF-1-NMDG. The initial Cr(VI) and As(V) concentrations in the testing solutions were 250 ppm. The equilibrium capacities of PAF-1-NMDG for both contaminants were reached by the first data points taken (10 s after the Cr(VI) and As(V) solutions were added). These nearly instantaneous adsorption kinetics are attributed to the high porosities, small particle sizes, and rapid binding mechanisms of PAF-1-NMDG.

our knowledge, these adsorption kinetics are the fastest of any reported adsorbent to date, for both chromium and arsenic.[4,9,56] The rapid adsorption rates of PAF-1-NMDG can be attributed largely to the high porosities, as indicated by relatively high surface areas (Figures S3 and S4), and small particle sizes (~200−250 nm diameter), as determined through FESEM (Figure S8), of this material, which minimize mass transfer resistances. Indeed, due to these properties, other functionalized PAF materials have likewise been reported to show among the fastest adsorption kinetics for their respective adsorbates.[17,20−22,57,58]

To understand how the unique Cr(VI) and As(V) oxyanion binding mechanisms of PAF-1-NMDG translate into selectivity over competing solutes, two-component adsorption selectivity experiments were conducted. Aqueous testing solutions were prepared by combining 2 mM solutions of either Cr(VI) or As(V) with 2, 20, or 200 mM (i.e., 1×, 10×, or 100× higher concentrations) solutions of Cl^-, NO_3^-, SO_4^{2-}, or $B(OH)_3$. As displayed in Figure 8, the measured PAF-1-NMDG Cr(VI) and As(V) adsorption capacities (q) for each solution were compared to the adsorption capacities measured for solutions devoid of competing constituents (q_0) (i.e., for solutions

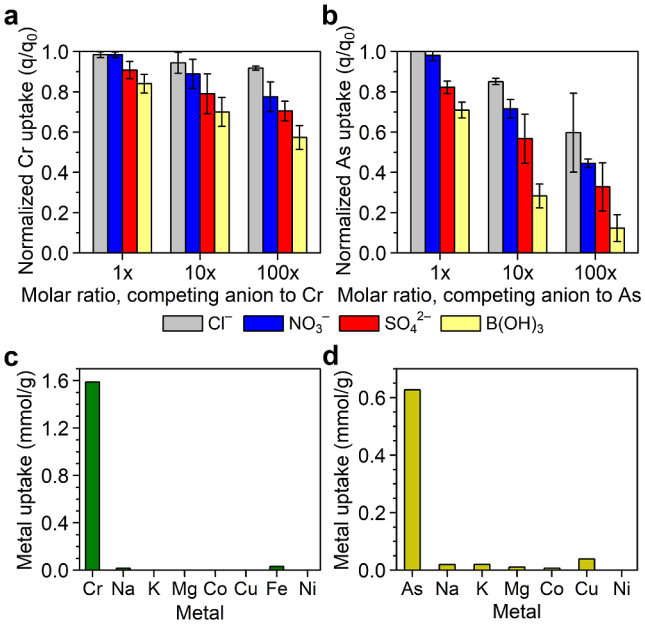

Figure 8. Two-component anion selectivity tests for PAF-1-NMDG at neutral conditions between (a) Cr(VI) or (b) As(V) and one type of the following competing constituents: NaCl (gray), $NaNO_3$ (blue), Na_2SO_4 (red), or $B(OH)_3$ (light yellow). In these tests, PAF-1-NMDG was mixed with a solution containing 2 mM of Cr(VI) or As(V), along with 2, 20 mM, or 200 mM of the competing constituent. q_0 denotes the equilibrium uptake for PAF-1-NMDG in a solution containing only 2 mM Cr(VI) or As(V) in DI water. Multicomponent metal selectivity tests for PAF-1-NMDG using solutions containing 2 mM of common competing metals and (c) Cr(VI) or (d) As(V). Error bars represent the standard deviation obtained from at least three replicate tests. The mean values obtained at each condition are shown.

containing only 2 mM Cr(VI) or As(V) in deionized water). Strong selectivity for As(V) and especially Cr(VI) by PAF-1-NMDG was observed in these measurements.

These selectivity tests revealed that Cr(VI) and As(V) adsorption is most negatively affected by competing solutes in the following order: $B(OH)_3 > SO_4^{2-} > NO_3^- > Cl^-$. The measurements also demonstrated that selectivity for Cr(VI) over other competing solutes is significantly higher than the As(V) selectivities, consistent with the unique polyol chelation and redox properties confirmed only for Cr(VI), along with the steeper adsorption isotherm profile observed for Cr(VI) (Figures 2−6). Importantly, PAF-1-NMDG shows excellent selectivity over Cl^-, which is the most abundant anion in many water streams.[59] For example, only 8% loss in Cr(VI) capacity was observed even in the presence of 200 mM Cl^-. The additional loss in Cr(VI) and As(V) capacity observed in the presence of NO_3^- and SO_4^{2-} was likely because the oxygen components of these competing anions can hydrogen-bond with the polyol functionalities, partially blocking Cr(VI) chelation and As(V) ion-exchange and hydrogen bonding with NMDG. Between these two competing anions, SO_4^{2-} decreases Cr(VI) and As(V) capacity more, likely because this anion possesses a higher charge and number of oxygen atoms, strengthening ion-exchange and hydrogen bonding interactions with NMDG.[60] The presence of $B(OH)_3$ decreased Cr(VI) and As(V) capacity the most of any competing solute due to the known ability of PAF-1-NMDG to chelate to $B(OH)_3$, as previously discussed.

https://doi.org/10.1021/jacs.4c05728
J. Am. Chem. Soc. 2024, 146, 23831−23841

We also explored the selectivity of PAF-1-NMDG for Cr(VI) and As(V) in the presence of common competing metal solutes. In these experiments, PAF-1-NMDG was mixed in solutions containing 2 mM of Cr(VI) or As(V) and 2 mM each of Na^+, K^+, Mg^{2+}, Cu^{2+}, Co^{2+}, Ni^{2+}, and Fe^{3+}. Solution pH was adjusted to 3 to ensure metal dissolution, and Fe^{3+} was omitted from the As(V) solution to avoid the precipitation of ferric arsenate. The results of these experiments show that PAF-1-NMDG displays excellent selectivity for Cr(VI) and As(V), adsorbing minimal amounts of competing metals (Figure 8c,d). This strong adsorption preference for Cr(VI) and As(V) can again be traced back to the unique binding interactions displayed by the NMDG functional group.

Since PAF-1-NMDG can selectively capture Cr(VI), As(V), and $B(OH)_3$, we performed three-component selectivity tests to better understand the PAF-1-NMDG adsorption selectivities between each solute. Aqueous solutions containing equimolar concentrations (0.2, 2, or 5 mM) of these three solutes were tested. Adsorption capacities in these experiments are provided in Figure S23, while Figure 9 displays the data in terms of selectivity (see also Section 1.10 in the Supporting Information). The results show that PAF-1-NMDG exhibits selectivity at neutral conditions in the approximate order: $B(OH)_3 \approx$ Cr(VI) > As(V) (Figure 9a). The higher selectivity achieved for Cr(VI) and $B(OH)_3$ over As(V) stems from the selective polyol chelation mechanisms observed for Cr(VI) and $B(OH)_3$, which leads to an increase in coordination number upon adsorption, whereas As(V) does not increase its number of bonds upon NMDG adsorption (as discussed above).

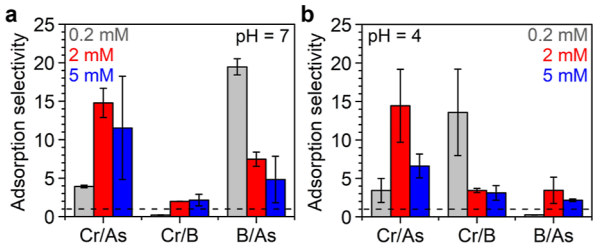

Figure 9. Equimolar three-component selectivity tests by PAF-1-NMDG for K_2CrO_7, KH_2AsO_4, and $B(OH)_3$, at (a) pH = 7 and (b) pH = 4 conditions as adjusted by HCl. The concentration of each species tested was 0.2 mM (gray), 2 mM (red), or 5 mM (blue). The dashed line indicates a value of unity, corresponding to no selectivity. Error bars represent the standard deviation obtained from at least three replicate tests. The mean values obtained at each condition are shown.

Notably, the total combined solute adsorption capacity by PAF-1-NMDG plateaus to a ~1:1 solute-to-NMDG ratio in these three-component experiments (Figure S21). This result suggests that each NMDG group cannot accommodate more than one solute at a time on average. This behavior corroborates previously proposed $B(OH)_3$ binding mechanisms that suggest that the amine is intrinsically linked to the polyol chelation, due to the ability of the amine to facilitate necessary proton transfer during the binding reaction between the NMDG O−H groups and the $B(OH)_3$ (or, here, CrO_4^{2-}) solute.[61]

The aforementioned three-component selectivity tests were also performed for PAF-1-NMDG under pH = 4 conditions. Selectivities from these experiments are given in Figure 9b, while Figure S23 displays the data in terms of adsorption capacity. The following selectivity order under these pH = 4 conditions differs from the pH = 7 data: Cr(VI) > $B(OH)_3 \approx$ As(V). Thus, adjusting the solution pH to slightly more acidic conditions (e.g., pH = 4) can be utilized to improve Cr(VI) and As(V) selectivity further. Acidic conditions are expected to improve Cr(VI) chelation to PAF-1-NMDG because the additional protons help drive the reduction of Cr(VI) to Cr(III).[62,63] The improved As(V) selectivity corroborates the stronger As(V) affinity observed in pH = 4 adsorption isotherms (Figure 3), likely due to the additional hydrogen bonding interactions and/or improved ease in chelating interactions, as previously discussed.

The improved Cr(VI) and As(V) selectivities observed under mildly acidic conditions also agree with other pH dependency tests. For example, two-component selectivity measurements revealed improved As(V) selectivity for PAF-1-NMDG over other competing solutes (Cl^-, NO_3^-, SO_4^{2-}, $B(OH)_3$) at pH = 4 conditions compared to pH = 7 conditions (Figure S22). We also tested the Cr(VI) and As(V) adsorption capacities of PAF-1-NMDG as a function of pH ranging from 1−12, using solutions containing 10 mg/L of either Cr(VI) or As(V) (Figures S15 and S16). Maximum capacities were attained under pH = 4 conditions for both adsorbates. Notably, minimal capacities were achieved under pH = 12 conditions. At these basic conditions, the NMDG groups ($pK_a \approx 9.6$)[64] are not expected to readily facilitate proton transfer in aqueous solution, and repulsive interactions between the oxyanions and deprotonated NMDG hydroxyl groups may additionally occur. These effects were similarly observed for $B(OH)_3$ capture under basic conditions.[22]

To maximize their lifetime and reduce capital costs, adsorbents must be capable of achieving regeneration over numerous cycles without facing significant performance loss or degradation. To this point, we tested the Cr(VI) and As(V) adsorption−desorption performances of PAF-1-NMDG over 10 cycles (Figure 10). Inspired by the desorption protocols used for desorbing chelated boron from NMDG groups,[22,52,53] we applied relatively mild acid and base washes (using 1 M HCl and 1 M NaOH) for the desorption of bound Cr and As(V) from PAF-1-NMDG. Remarkably, the adsorption capacity of PAF-1-NMDG for both Cr(VI) and As(V) remained constant even after 10 cycles. As further evidence

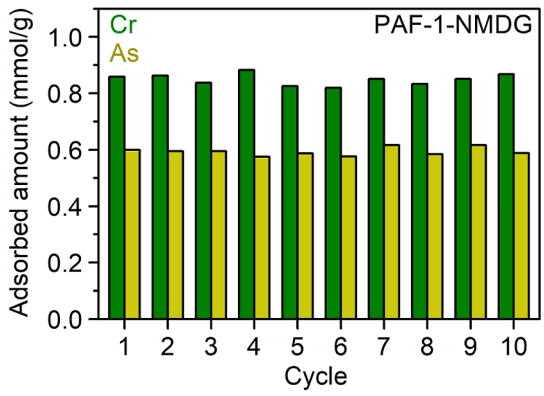

Figure 10. Regeneration and recyclability of PAF-1-NMDG for Cr(VI) (green) and As(V) (yellow). The adsorption solution contained 500 mg/L of Cr(VI) or As(V). Desorption was carried out using 1 M HCl and 1 M NaOH washes. No measurable loss in adsorption capacity for either toxic contaminant was observed over 10 adsorption−desorption cycles.

https://doi.org/10.1021/jacs.4c05728
J. Am. Chem. Soc. 2024, 146, 23831−23841

of this successful recycling, Cr-loaded PAF-1-NMDG displayed the characteristic green tint after every adsorption cycle, while reverting to its original light beige color after every desorption cycle (Figure S25). Retention of the chemical structure of PAF-1-NMDG during adsorption/desorption cycling was confirmed by FTIR and O 1s XPS, which indicated no framework or functional group degradation (Figures S38–S40). Notably, regeneration attempts using 1 M NaCl instead of 1 M HCl did not lead to appreciable Cr(VI) desorption from Cr-loaded PAF-1-NMDG (Figure S26). This finding validates the importance of acidic conditions to achieving desorption and further confirms that anion-exchange mechanisms are not primarily responsible for dilute Cr(VI) adsorption in PAF-1-NMDG. While the exact mechanisms of Cr desorption from PAF-1-NMDG are still under investigation, these results showcase the extraordinary reusability and stability of the PAF adsorbents.

To check whether the Cr(VI) and As(V) binding strategies utilized by PAF-1-NMDG could be applied more generally to other PAF materials, we synthesized an analogous material (P2-NMDG, see Figure 1a) consisting of longer terphenyl struts in the PAF backbone rather than biphenyl struts. Characterization data obtained for this material were similar to those of PAF-1-NMDG. For example, consistent with previous reports,[22] elemental analyses demonstrated that P2-NMDG possesses an NMDG loading of 2.36 mmol/g (Table S1) and a similar TGA decomposition profile (Figure S7). Adsorption isotherms for P2-NMDG showed highly similar Cr(VI) and As(V) properties compared to PAF-1-NMDG: ∼1:1 NMDG/Cr and ∼2:1 NMDG/As loadings and high K_L values of 17.7 and 1.9 L/mmol for Cr(VI) and As(V), respectively (Figures S12, S18, and S19 and Tables S2 and S3). Adsorption characteristics also suggested that P2-NMDG binds to these adsorbates in similar fashions to those by PAF-1-NMDG. To this point, Cr-loaded P2-NMDG displayed a green color and Cr K-edge XANES spectrum (Figure S34) practically identical to those of Cr-loaded PAF-1-NMDG (Figure 4a).

Comparisons to Other State-of-the-Art Materials. To provide context for the adsorption performance of PAF-1-NMDG, we investigated the adsorption performance of Amberlite IRA743 for comparison. This material is a commercial resin made up of NMDG-functionalized poly(styrene-divinylbenzene).[52] Adsorption isotherms of IRA743 for Cr(VI) and As(V) exhibited saturation capacities that were only 64.6 and 54.6% that of the Cr(VI) and As(V) saturation capacities, respectively, for PAF-1-NMDG (Figures S11, S18, and S19 and Tables S2 and S3). The higher loadings of PAF-1-NMDG are enabled by the higher NMDG loadings in these high-surface-area PAF materials (see Tables S2 and S3). The K_L values of IRA743 obtained for Cr(VI) (1.2) and As(V) (1.7) were also significantly lower than those observed for PAF-1-NMDG, suggesting more favorable binding by PAF-1-NMDG despite having the same NMDG functionality as IRA743. We note that a previous study from our laboratory similarly found that PAF-1-NMDG yields higher K_L values for $B(OH)_3$ adsorption compared to those obtained for IRA743.[22] Given the lower degree of synthetic control over the IRA743 pores compared to the highly tunable PAF micropores, we postulate that spacing between NMDG functional groups may be closer and more favorable in the PAF-1-NMDG materials, allowing strong bischelate interactions. Differences in the swelling behaviors of these materials may also contribute to the differences in their binding strengths.

We also tested the Cr(VI) and As(V) adsorption kinetics of IRA743 for comparison, using the same kinetics testing protocols as used for PAF-1-NMDG. The resin was first ball-milled to afford smaller particle sizes similar to those of PAF-1-NMDG, to diminish kinetics effects from particle size differences. For both oxyanions, the ball-milled IRA743 resin displayed markedly slower adsorption kinetics compared to PAF-1-NMDG (Figure S13). While PAF-1-NMDG reached equilibrium capacity within 10 s, IRA743 did not reach full equilibrium capacity until after 4 h, although by 30 min the resin did reach nearly 97 and 86% of the equilibrium capacities for Cr(VI) and As(V), respectively. The drastically faster adsorption kinetics for PAF-1-NMDG can be attributed to its much higher porosity, as previously described.

Tables S9 and S10 compare the Cr(VI) and As(V) adsorption performances, respectively, of PAF-1-NMDG more generally to the performances of other leading adsorbents. As previously mentioned, PAF-1-NMDG exhibits the fastest Cr(VI) and As(V) adsorption kinetics of any reported material to date, while maintaining high capacities on par with some of the highest-capacity materials. For example, other materials that achieve even higher capacities often take hours—even days—to reach their high equilibrium capacities. Unlike nearly all other materials, PAF-1-NMDG can additionally be recycled numerous times without any measurable loss in performance. It is worth noting that the majority of the other reports did not provide recyclability data, making further comparisons challenging. Importantly, with the exception of metal oxide materials used for As(V) removal, the vast majority of reported Cr(VI) and As(V) adsorbents also rely on simple ion-exchange mechanisms, which often face low selectivities not described in Tables S9 and S10. In contrast, PAF-1-NMDG features unique chelating and redox capabilities.

CONCLUSIONS

Chromium(VI)- and arsenic(V)-based oxyanions are among the most deleterious waterborne pollutants, plaguing communities worldwide whose water supplies are exposed to these toxic contaminants. The majority of adsorbents available for metal removal are applicable only for the removal of neutral or cationic pollutants, while those available for anionic pollutants most frequently rely on simple ion-exchange interactions that often offer low selectivity toward specific anions. In this work, we investigated the use of a series of amine- and aminopolyol-functionalized porous polymer frameworks for the targeted adsorption of Cr(VI) and As(V) oxyanions. Extensive adsorption experiments demonstrated that frameworks appended with NMDG functionalities can achieve high adsorption capacities, the fastest reported adsorption kinetics to date for Cr(VI) and As(V) binding, high selectivity over other common waterborne anions and metals, and recyclability using mild acid and base washes without measurable performance loss. Spectroscopic data (e.g., XAS and XPS spectra) and other systematic adsorption investigations (e.g., $B(OH)_3$ adsorption isotherms and pH dependency tests) indicated that this PAF-1-NMDG material achieves highly favorable Cr(VI) and As(V) binding through a combination of diol chelation, hydrogen bonding, ion exchange, and redox interactions. These investigations also showed that smaller aminopolyol groups (e.g., MAPD, serinol) do not offer the size and/or flexibility needed to achieve selective chelation mechanisms, offering important guidelines for the design of adsorbents for $B(OH)_3$ and $Si(OH)_4$ removal in addition to

https://doi.org/10.1021/jacs.4c05728
J. Am. Chem. Soc. 2024, 146, 23831−23841

Cr(VI) and As(V) removal. The favorable adsorption properties demonstrated for PAF-1-NMDG in this work altogether make this material highly promising for use in toxic chromium and arsenic oxyanion separations.

■ ASSOCIATED CONTENT

Supporting Information

The Supporting Information is available free of charge at https://pubs.acs.org/doi/10.1021/jacs.4c05728.

Additional experimental details, characterizations, adsorption data, results, and literature comparison data (PDF)

■ AUTHOR INFORMATION

Corresponding Author

Jeffrey R. Long − *Department of Chemical and Biomolecular Engineering, University of California, Berkeley, California 94720, United States; Materials Sciences Division, Lawrence Berkeley National Laboratory, Berkeley, California 94720, United States; Department of Chemistry, University of California, Berkeley, California 94720, United States;* orcid.org/0000-0002-5324-1321; Email: jrlong@berkeley.edu

Authors

Adam A. Uliana − *Department of Chemical and Biomolecular Engineering, University of California, Berkeley, California 94720, United States; Materials Sciences Division, Lawrence Berkeley National Laboratory, Berkeley, California 94720, United States;* Present Address: ChemFinity Technologies, Inc., Brooklyn, NY 11226, USA; orcid.org/0000-0002-2049-7240

Ethan R. Pezoulas − *Department of Chemistry, University of California, Berkeley, California 94720, United States;* orcid.org/0009-0006-4744-2668

N. Isaac Zakaria − *Department of Chemical and Biomolecular Engineering, University of California, Berkeley, California 94720, United States; Materials Sciences Division and Advanced Light Source, Lawrence Berkeley National Laboratory, Berkeley, California 94720, United States*

Arun S. Johnson − *Department of Chemical and Biomolecular Engineering, University of California, Berkeley, California 94720, United States; Materials Sciences Division, Lawrence Berkeley National Laboratory, Berkeley, California 94720, United States*

Alex Smith − *Department of Physics, University of California, Berkeley, California 94720, United States; Materials Sciences Division, Lawrence Berkeley National Laboratory, Berkeley, California 94720, United States*

Yubing Lu − *Molecular Biophysics and Integrated Bioimaging Division, Lawrence Berkeley National Laboratory, Berkeley, California 94720, United States*

Yusuf Shaidu − *Department of Physics, University of California, Berkeley, California 94720, United States;* orcid.org/0000-0001-9378-3910

Ever O. Velasquez − *Department of Chemical and Biomolecular Engineering, University of California, Berkeley, California 94720, United States; Materials Sciences Division, Lawrence Berkeley National Laboratory, Berkeley, California 94720, United States;* Present Address: ChemFinity Technologies, Inc., Brooklyn, NY 11226, USA.

Megan N. Jackson − *Materials Sciences Division, Lawrence Berkeley National Laboratory, Berkeley, California 94720, United States; Department of Chemistry, University of California, Berkeley, California 94720, United States;* Present Address: Department of Chemistry, University of North Carolina, Chapel Hill, NC 27599, USA.

Monika Blum − *Advanced Light Source, Lawrence Berkeley National Laboratory, Berkeley, California 94720, United States; Chemical Sciences Division, Lawrence Berkeley National Laboratory, Berkeley, California 94720, United States;* orcid.org/0000-0002-2918-9092

Jeffrey B. Neaton − *Department of Physics, University of California, Berkeley, California 94720, United States; Materials Sciences Division, Lawrence Berkeley National Laboratory, Berkeley, California 94720, United States; Kavli Energy NanoSciences Institute at Berkeley, Berkeley, California 94720, United States*

Junko Yano − *Molecular Biophysics and Integrated Bioimaging Division, Lawrence Berkeley National Laboratory, Berkeley, California 94720, United States;* orcid.org/0000-0001-6308-9071

Complete contact information is available at: https://pubs.acs.org/10.1021/jacs.4c05728

Funding

The synthesis of materials was supported by the National Alliance for Water Innovation (NAWI), funded by the U.S. Department of Energy, Office of Energy Efficiency and Renewable Energy (EERE), Industrial Efficiency and Decarbonization Office, under Funding Opportunity Announcement DE-FOA-0001905. Characterization efforts were funded by the U.S. Department of Energy, Office of Basic Energy Sciences, Separation Science in the Chemical Sciences, Geosciences, and Biosciences Division, under Award Number DE-SC0019992.

Notes

The authors declare the following competing financial interest(s): A.A.U., E.O.V., and J.R.L. have a financial interest in ChemFinity Technologies, Inc., a startup company developing selective sorbent materials for various chemical separations.

■ ACKNOWLEDGMENTS

We thank the U.S. National Science Foundation for providing graduate fellowship support for A.A.U. and E.O.V. and the Philomathia Foundation for providing additional graduate fellowship support for A.A.U. N.I.Z. was supported in part by an Advanced Light Source (ALS) Doctoral Fellowship in Residence and a National Defense Science & Engineering Graduate Fellowship, for which we thank the U.S. Department of Energy Office of Science and the U.S. Department of Defense, respectively. We are further thankful for the support of M.N.J. through an Arnold O. Beckman Postdoctoral Fellowship. High-energy X-ray absorption spectroscopy data were collected on beamline 10-BM at the Advanced Photon Source at Argonne National Laboratory, which is supported by U.S. Department of Energy, Office of Science, Office of Basic Energy Sciences under Contract no. DE-AC02-06CH11357. Dr. Mark Warren and Dr. Joshua Wright are thanked for assistance with XAS data collection. We also thank Dr. Elena Kreimer and the Microanalytical Facility for assistance with elemental analyses, ICP-OES measurements, and microbalance use. The University of California, Berkeley Electron Micro-

scope Laboratory is thanked for advice and assistance in electron microscopy sample preparation and data collection. We thank Dr. Mauricio Lopez Luna and Dr. Kaitlyn Engler for helpful discussions and Dr. Finn Babbe for instrument support. Dr. Isabel Bogacz is thanked for helpful discussions of X-ray absorption spectroscopy.

REFERENCES

(1) World Health Organization. *Progress on Drinking Water, Sanitation and Hygiene: 2017 Update and SDG Baselines*; United Nations Children's Fund, 2017.
(2) Werber, J. R.; Osuji, C. O.; Elimelech, M. Materials for Next-Generation Desalination and Water Purification Membranes. *Nat. Rev. Mater.* **2016**, *1* (5), 16018.
(3) Shannon, M. A.; Bohn, P. W.; Elimelech, M.; Georgiadis, J. G.; Mariñas, B. J.; Mayes, A. M. Science and Technology for Water Purification in the Coming Decades. *Nature* **2008**, *452* (7185), 301−310.
(4) Kumar, P.; Pournara, A.; Kim, K. H.; Bansal, V.; Rapti, S.; Manos, M. J. Metal-Organic Frameworks: Challenges and Opportunities for Ion-Exchange/Sorption Applications. *Prog. Mater. Sci.* **2017**, *86*, 25−74.
(5) Costa, M.; Klein, C. B. Toxicity and Carcinogenicity of Chromium Compounds in Humans. *Crit. Rev. Toxicol.* **2006**, *36* (2), 155−163.
(6) Dhal, B.; Thatoi, H. N.; Das, N. N.; Pandey, B. D. Chemical and Microbial Remediation of Hexavalent Chromium from Contaminated Soil and Mining/Metallurgical Solid Waste: A Review. *J. Hazard. Mater.* **2013**, *250*−*251*, 272−291.
(7) de Meyer, C. M. C.; Wahnfried, I.; Rodriguez Rodriguez, J. M.; Kipfer, R.; García Avelino, P. A.; Carpio Deza, E. A.; Berg, M. Hotspots of Geogenic Arsenic and Manganese Contamination in Groundwater of the Floodplains in Lowland Amazonia (South America). *Sci. Total Environ.* **2023**, *860*, 160407.
(8) Flanagan, S.; Johnston, R.; Zheng, Y. Arsenic in Tube Well Water in Bangladesh: Health and Economic Impacts and Implications for Arsenic Mitigation. *Bull. W. H. O.* **2012**, *90* (11), 839−846.
(9) Kobielska, P. A.; Howarth, A. J.; Farha, O. K.; Nayak, S. Metal Organic Frameworks for Heavy Metal Removal from Water. *Coord. Chem. Rev.* **2018**, *358*, 92−107.
(10) Bolisetty, S.; Peydayesh, M.; Mezzenga, R. Sustainable Technologies for Water Purification from Heavy Metals: Review and Analysis. *Chem. Soc. Rev.* **2019**, *48* (2), 463−487.
(11) Bhattacharyya, D.; Hestekin, J. A.; Brushaber, P.; Cullen, L.; Bachas, L. G.; Sikdar, S. K. Novel Poly-Glutamic Acid Functionalized Microfiltration Membranes for Sorption of Heavy Metals at High Capacity. *J. Membr. Sci.* **1998**, *141* (1), 121−135.
(12) Hestekin, J. A.; Bachas, L. G.; Bhattacharyya, D. Poly(Amino Acid)-Functionalized Cellulosic Membranes: Metal Sorption Mechanisms and Results. *Ind. Eng. Chem. Res.* **2001**, *40* (12), 2668−2678.
(13) Peng, H.; Guo, J. Removal of Chromium from Wastewater by Membrane Filtration, Chemical Precipitation, Ion Exchange, Adsorption Electrocoagulation, Electrochemical Reduction, Electrodialysis, Electrodeionization, Photocatalysis and Nanotechnology: A Review. *Environ. Chem. Lett.* **2020**, *18* (6), 2055−2068.
(14) Chen, G.; Feng, J.; Wang, W.; Yin, Y.; Liu, H. Photocatalytic Removal of Hexavalent Chromium by Newly Designed and Highly Reductive TiO_2 Nanocrystals. *Water Res.* **2017**, *108*, 383−390.
(15) Lin, Z.-J.; Zheng, H.-Q.; Zheng, H.-Y.; Lin, L.-P.; Xin, Q.; Cao, R. Efficient Capture and Effective Sensing of $Cr_2O_7^{2-}$ from Water Using a Zirconium Metal-Organic Framework. *Inorg. Chem.* **2017**, *56* (22), 14178−14188.
(16) Ben, T.; Ren, H.; Ma, S.; Cao, D.; Lan, J.; Jing, X.; Wang, W.; Xu, J.; Deng, F.; Simmons, J. M.; Qiu, S.; Zhu, G. Targeted Synthesis of a Porous Aromatic Framework with High Stability and Exceptionally High Surface Area. *Angew. Chem.* **2009**, *121* (50), 9621−9624.
(17) Tian, Y.; Zhu, G. Porous Aromatic Frameworks (PAFs). *Chem. Rev.* **2020**, *120* (16), 8934−8986.
(18) Demir, S.; Brune, N. K.; Van Humbeck, J. F.; Mason, J. A.; Plakhova, T. V.; Wang, S.; Tian, G.; Minasian, S. G.; Tyliszczak, T.; Yaita, T.; Kobayashi, T.; Kalmykov, S. N.; Shiwaku, H.; Shuh, D. K.; Long, J. R. Extraction of Lanthanide and Actinide Ions from Aqueous Mixtures Using a Carboxylic Acid-Functionalized Porous Aromatic Framework. *ACS Cent. Sci.* **2016**, *2* (4), 253−265.
(19) Uliana, A. A.; Bui, N. T.; Kamcev, J.; Taylor, M. K.; Urban, J. J.; Long, J. R. Ion-Capture Electrodialysis Using Multifunctional Adsorptive Membranes. *Science* **2021**, *372* (6539), 296−299.
(20) Lee, S.; Barin, G.; Ackerman, C. M.; Muchenditsi, A.; Xu, J.; Reimer, J. A.; Lutsenko, S.; Long, J. R.; Chang, C. J. Copper Capture in a Thioether-Functionalized Porous Polymer Applied to the Detection of Wilson's Disease. *J. Am. Chem. Soc.* **2016**, *138* (24), 7603−7609.
(21) Lee, S.; Uliana, A.; Taylor, M. K.; Chakarawet, K.; Bandaru, S. R. S.; Gul, S.; Xu, J.; Ackerman, C. M.; Chatterjee, R.; Furukawa, H.; Reimer, J. A.; Yano, J.; Gadgil, A.; Long, G. J.; Grandjean, F.; Long, J. R.; Chang, C. J. Iron Detection and Remediation with a Functionalized Porous Polymer Applied to Environmental Water Samples. *Chem. Sci.* **2019**, *10* (27), 6651−6660.
(22) Kamcev, J.; Taylor, M. K.; Shin, D. M.; Jarenwattananon, N. N.; Colwell, K. A.; Long, J. R. Functionalized Porous Aromatic Frameworks as High-Performance Adsorbents for the Rapid Removal of Boric Acid from Water. *Adv. Mater.* **2019**, *31* (18), 1808027.
(23) Ma, T.; Zhao, R.; Li, Z.; Jing, X.; Faheem, M.; Song, J.; Tian, Y.; Lv, X.; Shu, Q.; Zhu, G. Efficient Gold Recovery from E-Waste via a Chelate-Containing Porous Aromatic Framework. *ACS Appl. Mater. Interfaces* **2020**, *12* (27), 30474−30482.
(24) Polowczyk, I.; Urbano, B. F.; Rivas, B. L.; Bryjak, M.; Kabay, N. Equilibrium and Kinetic Study of Chromium Sorption on Resins with Quaternary Ammonium and N-Methyl-D-Glucamine Groups. *Chem. Eng. J.* **2016**, *284*, 395−404.
(25) Pan, Y.; Guan, D.-X.; Zhao, D.; Luo, J.; Zhang, H.; Davison, W.; Ma, L. Q. Novel Speciation Method Based on Diffusive Gradients in Thin-Films for in Situ Measurement of Cr(VI) in Aquatic Systems. *Environ. Sci. Technol.* **2015**, *49* (24), 14267−14273.
(26) Regan, J.; Huntington, D. C.; Capitani, J. F. Bidentate Reagents Form Cyclic Organic-Cr(VI) Molecules for Aiding in the Removal of Cr(VI) from Water: Density Functional Theory and Experimental Results. *Struct. Chem.* **2017**, *28* (5), 1461−1465.
(27) Urbano, B. F.; Rivas, B. L.; Martinez, F.; Alexandratos, S. D. Equilibrium and Kinetic Study of Arsenic Sorption by Water-Insoluble Nanocomposite Resin of Poly [N-(4-Vinylbenzyl)-N-Methyl-D-Glucamine]-Montmorillonite. *Chem. Eng. J.* **2012**, *193*−*194*, 21−30.
(28) Wei, Y.-T.; Zheng, Y.-M.; Chen, J. P. Enhanced Adsorption of Arsenate onto a Natural Polymer-Based Sorbent by Surface Atom Transfer Radical Polymerization. *J. Colloid Interface Sci.* **2011**, *356* (1), 234−239.
(29) Oliver, S. R. J. Cationic Inorganic Materials for Anionic Pollutant Trapping and Catalysis. *Chem. Soc. Rev.* **2009**, *38* (7), 1868−1881.
(30) Rapti, S.; Pournara, A.; Sarma, D.; Papadas, I. T.; Armatas, G. S.; Tsipis, A. C.; Lazarides, T.; Kanatzidis, M. G.; Manos, M. J. Selective Capture of Hexavalent Chromium from an Anion-Exchange Column of Metal Organic Resin-Alginic Acid Composite. *Chem. Sci.* **2016**, *7* (3), 2438.
(31) Li, X.; Xu, H.; Kong, F.; Wang, R. A Cationic Metal−Organic Framework Consisting of Nanoscale Cages: Capture, Separation, and Luminescent Probing of $Cr_2O_7^{2-}$ through a Single-Crystal to Single-Crystal Process. *Angew. Chem., Int. Ed.* **2013**, *52* (51), 13769−13773.
(32) BadertscherPretsch, M. E.; Bühlmann, P. *Structure Determination of Organic Compounds: Tables of Spectral Data*; Springer Berlin, Heidelberg, 2009.
(33) Lu, W.; Sculley, J. P.; Yuan, D.; Krishna, R.; Wei, Z.; Zhou, H. C. Polyamine-Tethered Porous Polymer Networks for Carbon Dioxide Capture from Flue Gas. *Angew. Chem., Int. Ed.* **2012**, *51* (30), 7480−7484.

https://doi.org/10.1021/jacs.4c05728
J. Am. Chem. Soc. 2024, 146, 23831−23841

(34) Alderighi, L.; Gans, P.; Ienco, A.; Peters, D.; Sabatini, A.; Vacca, A.; Simulation, H. Hyperquad Simulation and Speciation (HYSS): A Utility Program for the Investigation of Equilibria Involving Soluble and Partially Soluble Species. *Coord. Chem. Rev.* **1999**, *184* (1), 311−318.
(35) United States Environmental Protection Agency. *2018 Ed. Of the Drinking Water Standards and Health Advisories*; U.S. EPA: Washington, DC, 2018.
(36) Langmuir, I. The Adsorption of Gases on Plane Surfaces of Glass, Mica and Platinum. *J. Am. Chem. Soc.* **1918**, *40* (9), 1361−1403.
(37) Misak, N. Z. Langmuir Isotherm and Its Application in Ion-Exchange Reactions. *React. Polym.* **1993**, *21* (1−2), 53−64.
(38) Rapti, S.; Sarma, D.; Diamantis, S. A.; Skliri, E.; Armatas, G. S.; Tsipis, A. C.; Hassan, Y. S.; Alkordi, M.; Malliakas, C. D.; Kanatzidis, M. G.; et al. All in One Porous Material: Exceptional Sorption and Selective Sensing of Hexavalent Chromium by Using a Zr^{4+} MOF. *J. Mater. Chem. A* **2017**, *5* (28), 14707−14719.
(39) Gandhi, M. R.; Natrayasamy, V.; Meenakshi, S. Adsorption Mechanism of Hexavalent Chromium Removal Using Amberlite IRA 743 resin. *Ion. Exch. Lett.* **2010**, *3*, 25−35.
(40) Santander, I. P.; Urbano, B.; Leiton, L.; Yu, M. Removal of Cr(VI) by a Chelating Resin Containing N-Methyl-D-Glucamine. *Polym. Bull.* **2014**, *17*, 1813−1825.
(41) Goldberg, R. N.; Kishore, N.; Lennen, R. M. Thermodynamic Quantities for the Ionization Reactions of Buffers. *J. Phys. Chem. Ref. Data* **2002**, *31* (2), 231−370.
(42) Cassone, G.; Chillé, D.; Foti, C.; Giuffré, O.; Ponterio, R. C.; Sponer, J.; Saija, F. Stability of Hydrolytic Arsenic Species in Aqueous Solutions: As^{3+} vs. As^{5+}. *Phys. Chem. Chem. Phys.* **2018**, *20* (36), 23272−23280.
(43) Camacho, L. M.; Gutiérrez, M.; Alarcón-Herrera, M. T.; Villalba, M. d. L.; Deng, S. Occurrence and Treatment of Arsenic in Groundwater and Soil in Northern Mexico and Southwestern USA. *Chemosphere* **2011**, *83* (3), 211−225.
(44) Tsuyumoto, I.; Maruyama, Y. X-ray Fluorescence Analysis of Hexavalent Chromium Using Kβ Satellite Peak Observed as Counterpart of X-ray Absorption Near-Edge Structure Pre-Edge Peak. *Anal. Chem.* **2011**, *83* (19), 7566−7569.
(45) Frommer, J.; Nachtegaal, M.; Czekaj, I.; Weng, T. C.; Kretzschmar, R. X-Ray Absorption and Emission Spectroscopy of CrIII (Hydr)Oxides: Analysis of the K-Pre-Edge Region. *J. Phys. Chem. A* **2009**, *113* (44), 12171−12178.
(46) Smith, P. G.; Koch, I.; Gordon, R. A.; Mandoli, D. F.; Chapman, B. D.; Reimer, K. J. X-ray Absorption Near-Edge Structure Analysis of Arsenic Species for Application to Biological Environmental Samples. *Environ. Sci. Technol.* **2005**, *39* (1), 248−254.
(47) Biesinger, M. C.; Brown, C.; Mycroft, J. R.; Davidson, R. D.; McIntyre, N. S. X-Ray Photoelectron Spectroscopy Studies of Chromium Compounds. *Surf. Interface Anal.* **2004**, *36* (12), 1550−1563.
(48) Yashin, V. A.; Os'mushko, I. S.; Vovna, V. I.; Korochentsev, V. V.; Shapkin, N. P.; Tutov, M. V. Electronic Structure of Chromium-(III) Acetylacetonate Sulfenyl Chloride and Its γ-Vinyltrimethylsilane-Substituted Derivatives According to XPS and DFT Data. *Russ. J. Inorg. Chem.* **2022**, *67* (9), 1433−1441.
(49) McMurry, J. E. *Organic Chemistry with Biological Applications*; Cengage Learning, 2014.
(50) Morosin, B. The Crystal Structure of Trisacetylacetonatochromium(III). *Acta Crystallogr.* **1965**, *19* (1), 131−137.
(51) Ruben, H.; Olovsson, I.; Zalkin, A.; Templeton, D. H.; Tetrahydrate, S. C. Sodium Chromate Tetrahydrate. *Acta Crystallogr., Sect. B: Struct. Crystallogr. Cryst. Chem.* **1973**, *29* (12), 2963−2964.
(52) Hilal, N.; Kim, G. J.; Somerfield, C. Boron Removal from Saline Water: A Comprehensive Review. *Desalination* **2011**, *273* (1), 23−35.
(53) Guler, E.; Kaya, C.; Kabay, N.; Arda, M. Boron Removal from Seawater: State-of-the-Art Review. *Desalination* **2015**, *356*, 85−93.
(54) Yoshimura, K.; Miyazaki, Y.; Ota, F.; Matsuoka, S.; Sakashita, H. Complexation of Boric Acid with the N-Methyl-D-Glucamine Group in Solution and in Crosslinked Polymer. *J. Chem. Soc., Faraday Trans.* **1998**, *94* (5), 683−689.
(55) Salvador Cob, S.; Hofs, B.; Maffezzoni, C.; Adamus, J.; Siegers, W.; Cornelissen, E.; Genceli Güner, F.; Witkamp, G. Silica Removal to Prevent Silica Scaling in Reverse Osmosis Membranes. *Desalination* **2014**, *344*, 137−143.
(56) Li, P.; Damron, J. T.; Bryantsev, V. S.; Johnson, K. R.; Stamberga, D.; Mahurin, S. M.; Popovs, I.; Jansone-Popova, S. Guanidinium-Based Ionic Covalent-Organic Nanosheets for Sequestration of Cr(VI) and As(V) Oxoanions in Water. *ACS Appl. Nano Mater.* **2021**, *4* (12), 13319−13328.
(57) Li, B.; Zhang, Y.; Ma, D.; Shi, Z.; Ma, S. Mercury Nano-Trap for Effective and Efficient Removal of Mercury(II) from Aqueous Solution. *Nat. Commun.* **2014**, *5* (1), 5537.
(58) Yuan, Y.; Yang, Y.; Ma, X.; Meng, Q.; Wang, L.; Zhao, S.; Zhu, G. Molecularly Imprinted Porous Aromatic Frameworks and Their Composite Components for Selective Extraction of Uranium Ions. *Adv. Mater.* **2018**, *30*, 12.
(59) Landsman, M. R.; Sujanani, R.; Brodfuehrer, S. H.; Cooper, C. M.; Darr, A. G.; Davis, R. J.; Kim, K.; Kum, S.; Nalley, L. K.; Nomaan, S. M.; Oden, C. P.; Paspureddi, A.; Reimund, K. K.; Rowles, L. S.; Yeo, S.; Lawler, D. F.; Freeman, B. D.; Katz, L. E.; Treatment, W. Water Treatment: Are Membranes the Panacea? *Annu. Rev. Chem. Biomol. Eng.* **2020**, *11* (1), 559−585.
(60) Luo, T.; Abdu, S.; Wessling, M. Selectivity of Ion Exchange Membranes: A Review. *J. Membr. Sci.* **2018**, *555* (December 2017), 429−454.
(61) Nasef, M. M.; Nallappan, M.; Ujang, Z. Polymer-Based Chelating Adsorbents for the Selective Removal of Boron from Water and Wastewater: A Review. *React. Funct. Polym.* **2014**, *85*, 54−68.
(62) Stern, C. M.; Abeythunga, M. M.; Elgrishi, N. Advancing Cr(VI) Electroreduction: A Redox Mediator to Catalyze the Electrochemical Reduction of Cr(VI) in Water While Preventing Fouling of Carbon Electrodes. *ACS Org. Inorg. Au* **2023**, *4* (6), 113−119.
(63) Fang, L.; Zeng, J.; Wang, H.; He, F.; Wan, H.; Li, M.; Ren, W.; Ding, L.; Yang, L.; Luo, X. Insights into the Proton-Enhanced Mechanism of Hexavalent Chromium Removal by Amine Polymers in Strong Acid Wastewater: Reduction of Hexavalent Chromium and Sequestration of Trivalent Chromium. *J. Colloid Interface Sci.* **2023**, *650*, 515−525.
(64) Settimo, L.; Bellman, K.; Knegtel, R. M. A. Comparison of the Accuracy of Experimental and Predicted PKa Values of Basic and Acidic Compounds. *Pharm. Res.* **2014**, *31* (4), 1082−1095.

https://doi.org/10.1021/jacs.4c05728
J. Am. Chem. Soc. 2024, 146, 23831−23841